

CrystEngComm

Accepted Manuscript



This is an *Accepted Manuscript*, which has been through the Royal Society of Chemistry peer review process and has been accepted for publication.

Accepted Manuscripts are published online shortly after acceptance, before technical editing, formatting and proof reading. Using this free service, authors can make their results available to the community, in citable form, before we publish the edited article. We will replace this *Accepted Manuscript* with the edited and formatted *Advance Article* as soon as it is available.

You can find more information about *Accepted Manuscripts* in the [Information for Authors](#).

Please note that technical editing may introduce minor changes to the text and/or graphics, which may alter content. The journal's standard [Terms & Conditions](#) and the [Ethical guidelines](#) still apply. In no event shall the Royal Society of Chemistry be held responsible for any errors or omissions in this *Accepted Manuscript* or any consequences arising from the use of any information it contains.

Evolutionary Growth of Microscale Single Crystalline GaN on Amorphous Layer by Combination of MBE and MOCVD

Cite this: DOI: 10.1039/x0xx00000x

Received 00th January 2012,
Accepted 00th January 2012

DOI: 10.1039/x0xx00000x

www.rsc.org/crystengcomm

Jung-Wook Min,^a Si-Young Bae,^b Won-Mo Kang,^c Kwang Wook Park,^d
Eun-Kyu Kang,^e Bong-Joong Kim,^c Dong-Seon Lee^{*e} Yong-Tak Lee^{*de}

To integrate multiple functional devices on a chip, advances in epitaxial growth on heterosubstrates are required. As one approach to achieve an epitaxial layer on an amorphous substrate, we developed a method of combined epitaxial growth using molecular beam epitaxy (MBE) and metal-organic chemical vapor deposition (MOCVD). This two-stage combined growth can be used to grow a binary gallium nitride (GaN) on any thermally durable substances. The first MBE growth step provided us effective nucleation with uniform morphology. Meanwhile, the second MOCVD growth enabled improved crystalline quality. Detailed analysis at grain-to-grain and layer-to-layer interfaces was studied with high-resolution transmission electron microscopy (TEM) characterization. This study gives a deep understanding of the growth behavior, thereby supporting the demonstration of perfect single crystalline GaN, enabling the realization of optoelectronic GaN-based devices on amorphous layer.

Introduction

GaN-based heteroepitaxy growth techniques have been successfully established in solid-state optoelectronics since the first demonstration of high brightness LEDs.^{1,2} Nowadays, high quality GaN can be grown on Si substrate with promoting large-scale GaN epitaxy on substrates over 8-inches in size, resulting in high chip yields with low cost.³ However, the strong light absorption by the Si substrate over the entire visible wavelength range is one of the critical drawbacks to its application in visible light-emitting devices.⁴ In efforts to address the unfavorable properties of the Si substrate, several research groups have reported vertical light-emitting diodes (LEDs) with a Si substrate removal process. To overcome the limit of the existing substrate and to explore novel applications, various alternative substrates have been investigated, such as reflective metallic substrates, e.g. Ag, Cu, W, Ta, Mo, and Nb etc. or transparent amorphous substrates, e.g. diamond, quartz, fused silica and so on.^{5–8} So far, few investigations have reported the direct growth of GaN on amorphous substrates via MOCVD since the directly grown GaN typically results in weakly preferred orientations and rough morphologies due to absence of proper assistant buffer materials.^{7,9} The majority of efforts to grow GaN on amorphous substrates have been attempted using electron cyclotron resonance molecular beam epitaxy (ECR-MBE).^{6,8} The ECR cell provides remarkably

enhanced N₂ reactivity in forming a GaN layer on amorphous surfaces, and the ECR cell-assisted nitridation process in the initial stage improves both crystal quality and surface morphology.^{10,11} However, ECR-MBE grown GaN exhibits poor crystal quality due to excessively high plasma power.¹² On the other hand, there is another alternative, called radio frequency plasma-assisted MBE (PA-MBE), which allows atomic-scale molecular beam epitaxy growth under low growth temperature and following high quality epitaxy. It also enables sub-microscale polycrystalline grains of highly *c*-plane oriented GaN on amorphous substrates.^{11,13} Owing to the Volmer-Weber (VW) dominant growth mode under the high V/III flux ratio of the N-rich condition, coalesced GaN columns can be formed as a pre-orienting layer with enhanced growth uniformity.^{6,8,11} Another advantage of PA-MBE is the easy polarity-based control of surface orientation, as either +*c*-plane orientation (Ga-polarity) or –*c*-plane orientation (N-polarity). In these processes, a conventional Ga-polar GaN layer is introduced by a high-temperature AlN buffer layer and nitridation process on an Al containing substrate, while an N-polar GaN layer is predominantly induced without an Al platform.¹⁴ In particular, the availability of N-polar GaN is a noteworthy feature since it gives a reverse spontaneous polarization along the direction opposite to Ga-polar GaN, thereby inducing a significant change in the energy band profiles of a heterojunction.¹⁵ Furthermore, tailoring the band profile using an N-polar GaN

layer has application in several kinds of electronic/optoelectronic devices, e.g., field-effect transistors (FET) using altered two-dimensional gases at the GaN/AlGaIn interface, InGaIn-based solar cells with reduced piezoelectric polarization, and highly efficient LEDs with high indium incorporation as well as reduced efficiency droop.^{16–18}

On the other hand, there have been still several attempts to grow GaN on substitute substrates using MOCVD. Recently Choi et al. reported an LED structure grown on an amorphous substrate.¹⁹ To improve the preferred orientation and crystalline quality, Choi et al. applied a Ti seed layer as a pre-orienting layer. After formation of the preferred orientation, low temperature GaN and high temperature local GaN growth were performed sequentially, using a SiO₂ mask layer on micro-sized openings via MOCVD.¹⁹ This suggested an easy method to tune the aspect ratio of locally grown GaN simply by changing the growth condition.²⁰ And there is still room, by optimizing the SiO₂ mask opening size, to achieve the maximum crystalline quality of the local epitaxy. In the MOCVD system, it is difficult to obtain an optimized mask opening size due to the grain roughness beneath the SiO₂ mask layer. The grain roughness of MOCVD grown GaN is microscale, which is comparable to the size of the mask openings.⁷ Also, it is not easy to avoid these obstacles due to the nature of MOCVD growth.⁹ However, the MBE growth technique can induce a high density of grains within the polycrystalline layer, whilst,

the grain size become limited to nanometer-scale with fairly uniform size distribution.¹³ This small size of grains can be advantageous for optimizing the mask opening size. At present, however, little attention has been given to a structural analysis of the grains.

In this work, we investigated the distribution of grain size and their material properties at each interface before determination of the proper scale of local epitaxy. As an intermediate stage, this study tried to provide a deep understanding of GaN growth behavior on amorphous layer. Furthermore, in order to easily achieve high quality GaN growth on a substitute substrate, we applied a combined growth technique: PA-MBE growth (1st GaN), followed sequentially by MOCVD growth (2nd GaN). In the combined growth technique, an amorphous layer was applied as a substitute intermediation layer when growing the PA-MBE grown polycrystalline GaN layer, to obtain a highly $\pm c$ -oriented GaN layer. As the amorphous layer, we adopted Si₃N₄ grown on quartz plate. Thermal expansion coefficient of Si₃N₄ is between GaN and quartz, so detrimental stress to GaN layer can be reduced during cooling process. Additionally, it is noteworthy that the Si₃N₄ layer is easily able to be deposited on any kind of thermally durable substrate.

Experimental

1st GaN growth (MBE) procedure

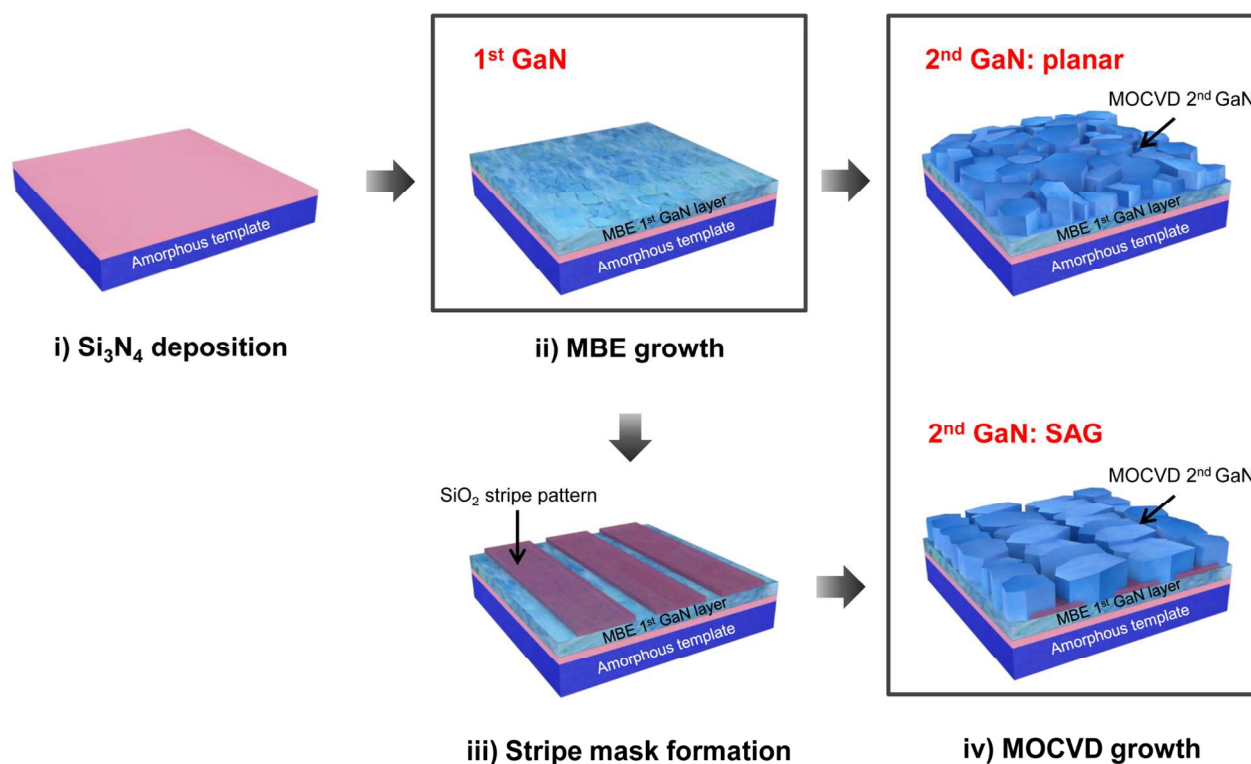


Fig. 1. Schematic of the growth procedure for (i) Si₃N₄ deposition on quartz wafer, (ii) 1st GaN layer growth via MBE, (iii) SiO₂ stripe mask formation via PECVD, and (iv) 2nd GaN layer growth via MOCVD. Planar growth was performed on bare 1st GaN template without mask formation (up) and SAG was performed on stripe patterned surface of 1st GaN (down).

Prior to epitaxial layer growth, a 500-nm-thick Si_3N_4 layer was deposited on a quartz substrate using plasma enhanced chemical vapor deposition (PECVD). As precursors for reaction, NH_3 and SiH_4 gases are introduced to PECVD chamber and subsequently Si_3N_4 layer is deposited at 300°C . Next, pieces of Si_3N_4 /quartz samples ($\sim 5\text{ cm}^2$) were mounted on molybdenum block using the indium paste method, and the block was loaded into preparation chamber of modified PA-MBE (VG-V80). After pre-outgas of the sample mounted molybdenum block at 300°C for 30 min in the preparation chamber, the sample was transferred to the growth chamber and thermally cleaned at 900°C for 30 min to remove residual native oxide on the sample surface. Next, the nitridation process and the following 1st GaN layer growth were performed on the Si_3N_4 layer in a PA-MBE growth chamber equipped with an RF plasma source (Arios IRFS 504) and in-situ reflection high-energy electron diffraction (RHEED) at 20 kV. The 1st GaN layer was grown for 1 hour at 700°C with plasma atmosphere generated under 350 W of RF power and 1.0 sccm of N_2 . By ramping the growth temperature up to 800°C , 3×10^{-7} mBar of Ga beam equivalent pressure (BEP) was introduced to the sample without any buffer layer. With the growth process, a 700 nm thick polycrystalline GaN was grown, and the chamber pressure was kept at around 3.5×10^{-5} mbar. During the MBE growth, RHEED (Arios 201) analysis technique was applied to obtain in-situ monitoring of the GaN layer quality and orientation.

2nd GaN growth (MOCVD) procedure

After completing the 1st GaN layer growth using MBE, the sample was transferred to the MOCVD reactor (MO260S-Sysnex, Korea) for the 2nd GaN layer growth. In this step, the 2nd GaN layer was grown not only on the bare surface (planar 2nd GaN) but also the patterned surface of the 1st GaN layer using selective area growth (SAG- 2nd GaN). To form the patterned surface on the 1st GaN surface, a stripe-patterned (window-/mask length = $3\ \mu\text{m}/3\ \mu\text{m}$) SiO_2 mask was formed; first, a 200 nm thick SiO_2 layer was deposited on the 1st GaN layer by PECVD and then, the stripe openings for SAG were defined by photolithography technique and etched by reactive ion etching (RIE) using CF_4/O_2 gases. The samples were heated to 1050°C at 13.3 kPa under ambient hydrogen (H_2). As soon as the growth temperature reached 450°C , ammonia (NH_3) was injected to reduce the thermal dissociation of the 1st GaN layer. For the synthesis of the 2nd GaN layer, flow rates of the trimethylgallium (TMGa) and NH_3 were maintained at 100 sccm ($165.5\ \mu\text{mol}/\text{min}$) and 8 slm ($357.1\ \text{mmol}/\text{min}$), respectively. Growth duration of the 2nd GaN layer was kept at 45 min.

Fig. 1 illustrates the combined epitaxy growth procedure with MBE and MOCVD. To eliminate any unpredictable factors during the 2nd GaN layer growth step, both the planar 2nd GaN layer growth and the SAG- 2nd GaN layer were performed at the same time in the MOCVD reactor to study the growth features under the same condition.

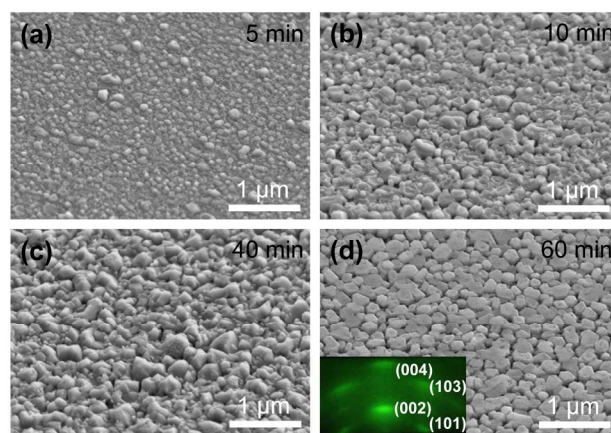


Fig. 2. SEM images of PA-MBE grown 1st GaN surfaces on the amorphous Si_3N_4 layer by the growth time of (a) 5 min, (b) 10 min, (c) 40 min, and 60 min. Inset of Fig. 2(d) is the in-situ RHEED pattern during MBE growth, where polycrystalline orientation of the 1st GaN was reflected. As growth time elapses, the size of nanoclusters enlarged and the surface was almost fully covered by these nanoclusters.

Sample treatment and characterization

To investigate the polarity of the 2nd GaN layer, 3M KOH etching solution was prepared. The SAG- 2nd GaN sample was dipped into the 80°C KOH solution for 5 min. The surface morphology and atomic intensity was investigated by field-emission scanning electron microscopy with energy dispersive X-ray (EDX) analysis (FE-SEM, Hitachi S-4700 EMAX). To investigate the structural properties of the grown GaN layers as well as the amorphous layer, transmission electron microscopy (TEM, Technai G² F30 S-Twin) was carried out to obtain bright-field (BF) images, high-resolution (HR) images, and selected area diffraction (SAD) pattern at the interfaces. For the TEM measurement, samples were sliced by a dual-beam focus ion beam (DB-FIB, NOVA 200). The crystal orientations and crystalline quality of the grown samples were evaluated by X-ray diffraction (XRD, Panalytical X'Pert pro). Further optical properties were characterized by photoluminescence (PL) and cathodoluminescence (CL, MONO CL3+) which was used to perform spatial emission mapping and spot-mode spectra measurement.

Results and Discussion

I. Growth evolution of 1st GaN on PA-MBE

In order to find the initial growth behavior on the amorphous Si_3N_4 layer during PA-MBE procedure, we grew the samples by changing growth time. Fig. 2 presents the SEM images of the sample surfaces for the growth time from 5 min to 60 min. We could observe the droplet-like nanoclusters were formed on the surface at the beginning (Fig. 2(a)). As growth time elapses, the size of nanoclusters enlarged and the surface was almost fully covered by these nanostructures (Fig. 2(b) and 2(c)). Finally, it has closely packed hundreds-of-nanometer-sized columnar grains with a randomly twisted in-plane direction (Fig.

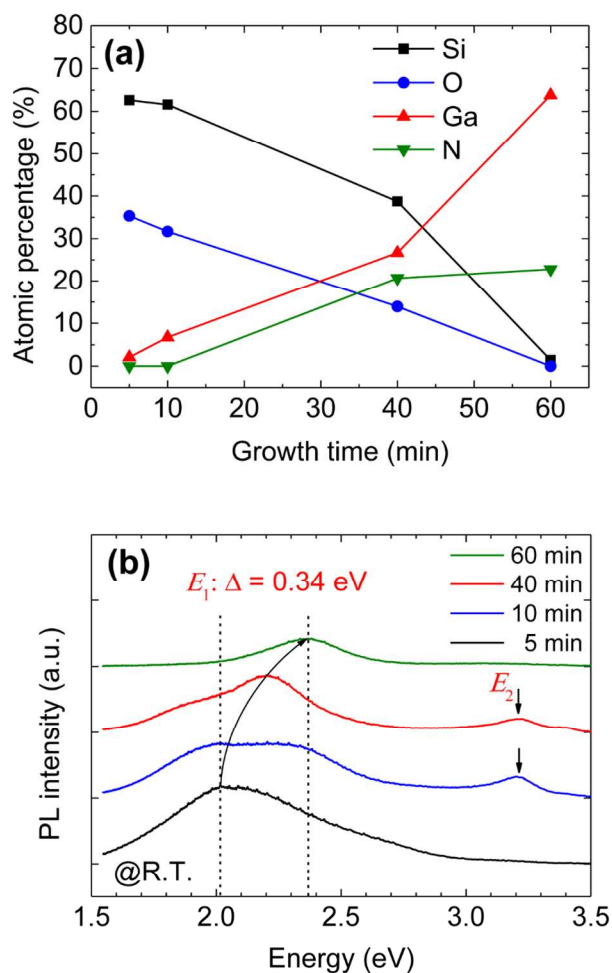


Fig. 3. (a) EDX characterization and (b) room temperature PL measurement of 1st GaN by increasing growth time of 5 min, 10 min, 40 min, and 60 min. Initial nucleation was mainly attributed to the GaO_x alloy nanoclusters and main peak (E_1) was blueshifted by 0.34 eV as growth time increases up to 60 min.

2(d)). At the same time, we monitored RHEED pattern during MBE growth via an in-situ RHEED gun mounted on the chamber, as shown in the inset of Fig. 2(d). Whilst no distinguished pattern were observed during nitridation and early growth process (not shown), disconnected ring-like patterns appeared in the 1st GaN grown during 60 min. Bright spots in the RHEED pattern corresponds to the (002), (004), (101), and (103) orientations, thereby indicating polycrystalline nature.²¹ Note that MOCVD epitaxy on the lattice mismatched substrate (and/or amorphous layer) typically results in random distribution of nucleated three dimensional (3D) bulky GaN, i.e., it is quite difficult to grow a GaN film which covers the whole amorphous surface.²² To understand the mechanism behind the full surface coverage achieved with the MBE grown GaN layer, we firstly performed the EDX characterization for each samples (Fig. 3(a)). Surprisingly, N atoms were not detected at the beginning of growth, but only Ga and O atoms were observed (5 min and 10 min). It means that initial

nucleation was mainly attributed to the GaO_x alloy nanoclusters. As the growth time elapses, N atoms start to be detected, whilst O atoms were slowly vanished (40 min and 60 min). We believe that these O atoms were originated from native oxide on the sample surface. The monotonic decrease of Si atoms was attributed to intensity weakening of EDX signal from upper structure thicker. Hence, the formation of GaO_x nanoclusters might perform a key role as nucleation region to grow the upper columnar GaN structure. To prove the role of GaO_x nanostructures, we further implemented PL measurement on these samples with He-Cd laser in Fig. 3(b). One main peak (E_1) was found at 2.02 eV for 5 min sample and it was blueshifted by 0.34 eV as growth time increases up to 60 min, whereas the other satellite peak was located at 2.36 eV for 10-min and 40-min samples. It is speculated that the origin of these E_1 and E_2 peaks from the stoichiometric variation of (Ga₂O₃)_n clusters (n = 1–10) as theoretically reported elsewhere.²³ In addition, the remarkable blueshifting behavior of E_1 is quite well matched with the size effect of Ga₂O₃ nanostructures.²⁴

II. Growth morphology of 2nd GaN via MOCVD

As for the next step of 1st GaN growth, 2nd GaN growth was implemented on MOCVD. Fig. 4 displays the SEM images of planar 2nd GaN grown for 15 min (Fig. 4(a) and 4(b)) and 45 min (Fig. 4(c) and 4(d)). It shows microscale platelet-shaped grains larger than the ones found in the 1st GaN layer. The size of these platelet-shaped grains was enlarged as an angle difference between one grain and adjacent grain become smaller. As can be seen in Fig 4(b), for example, G1 and G2 compose rather enlarged planar grains with small angle difference ($\Delta\theta_1$), whereas abrupt distortion was formed at interface between G2 and G3 with large angle difference ($\Delta\theta_2$). The increased growth time induces much more chances where the grains meet the other grains with larger angle difference, thereby planar grains get reduced and 3D microstructures

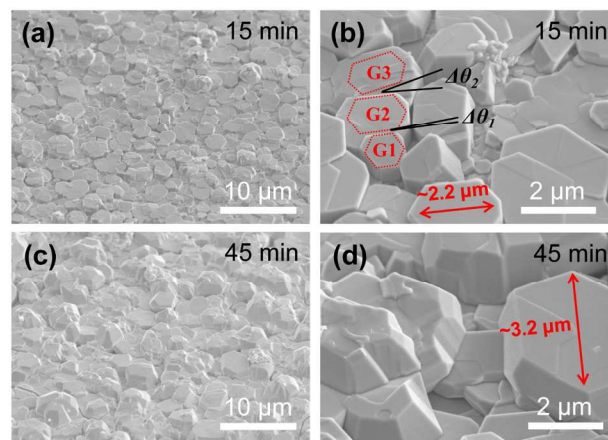


Fig. 4. SEM images of (a) planar 2nd GaN grown for 15 min, (b) its zoomed image of microscale platelet-shaped grains, (c) planar 2nd GaN grown for 45 min, and (d) its zoomed image for enlarged planar grains.

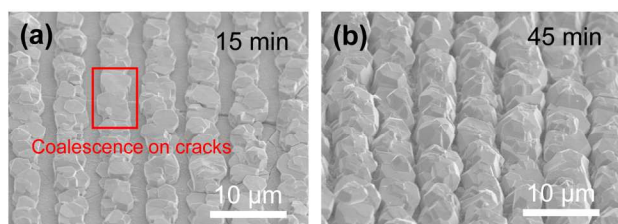


Fig. 5. SEM images of (a) SAG- 2nd GaN grown by MOCVD for 15 min and (b) 45 min. Controlled morphology along the stripe window was achieved and grain size became two times larger than that of the planar 2nd GaN (fig. 4(b) and 4(d)).

became dominant, as shown in Fig. 4(c). Nevertheless, some particular planar grains could be grown by the grain size of $\sim 3.2 \mu\text{m}$, as shown in Fig. 4(d). Hence, the coherency of edge angle between grain-to-grain is quite important to evolve the two dimensional (2D) layer.

To reduce the chances that the microscale grains meet with neighbors, we performed SAG with a stripe-shaped mask, thereby reducing the degree of freedom on the in-plane growth

direction by half (Fig. 5). As a result, controlled morphology along the stripe window was achieved and the platelet-shaped grain size became approximately two times larger than that of the planar 2nd GaN. Furthermore, some cracks observed on the 1st GaN layer were covered by coalescence above crack boundaries, as shown in Fig. 5(a). It indicates that microstructural dislocations could be reduced by strong lateral growth. The average growth rate of the planar 2nd GaN layer was $\sim 5 \mu\text{m/h}$ and this is larger than twice of the one obtained by typical planar GaN on sapphire ($\sim 2.2 \mu\text{m/h}$) under the same growth condition, indicating that vertical growth was enhanced by island-like Stranski–Krastanov (SK) mode growth. In contrast, the SAG- 2nd GaN layer had a slightly reduced growth rate of $\sim 4.4 \mu\text{m/h}$, indicating enhancement of lateral growth. However, the striped-SAG also results in distorted 3D microstructures as growth time increase due to the competition of individual grains which still have twisted preferred orientation along in-plane direction (Fig. 5(b)).

III. Microstructural TEM analysis

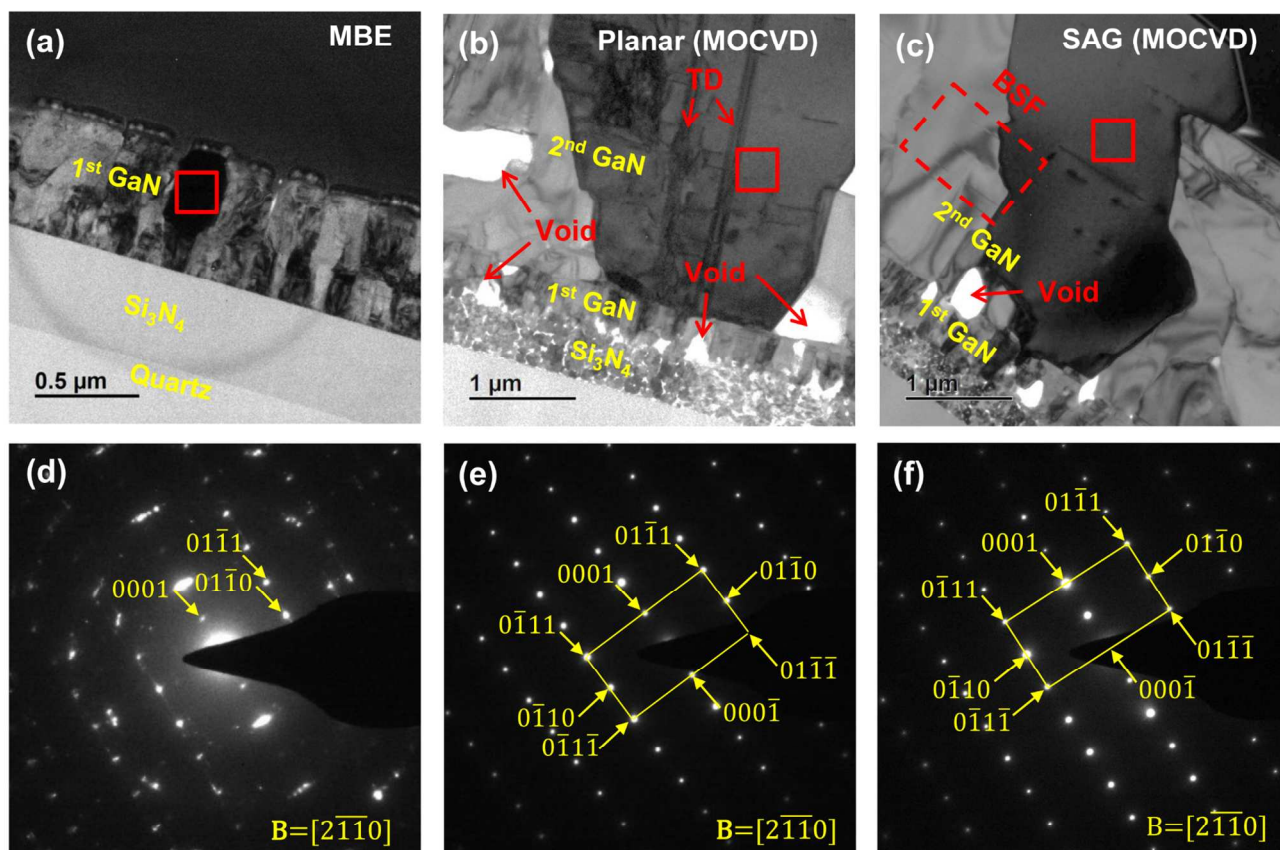


Fig. 6. Cross-sectional dark-field TEM images of (a) 1st GaN, (b) planar 2nd GaN, and (c) SAG- 2nd GaN. Their corresponding SAD patterns are shown in Fig. 6(d)–(f), respectively. The high density of defects including TD in the planar 2nd GaN was reduced by SAG. Each microscale grain has single GaN crystallinity within the middle of grain.

In order to study the structural properties of the grown layers, TEM analysis was carried out. Fig. 6(a)–6(c) are dark-field (DF) TEM images taken from the 1st GaN layer, the planar 2nd GaN layer, and the SAG- 2nd GaN layer, respectively. In Fig. 6(a), the cross-sectional view shows that the 1st GaN layer is composed of a few hundreds-of-nanometer columnar grains on the amorphous Si₃N₄ layer. Typically it shows heights of ~700 nm and diameters of ~250 nm. On the other hand, the MOCVD growth apparently induced much enlarged grains of a few micrometer-size on the planar 2nd GaN layer and SAG- 2nd GaN layer (Fig. 6(b) and 6(c)). The grain enlargement is believed to be mainly caused by the long surface diffusion length of adatoms and the altered growth mode via MOCVD. In particular, the 250°C higher growth temperature of the MOCVD compared to MBE affected the Si₃N₄ layer, thereby results in deformation and re-crystallization of the amorphous Si₃N₄ layer (Fig. 6(b) and 6(c)), while the Si₃N₄ layer did not suffer any deformation during the 1st GaN growth step (Fig. 6(a)). Note that this is not surprising considering that the GaN layers were often grown on a few nanometers of Si₃N₄ layer to reduce the TDs for the GaN/Si.²⁵ In other words, this can easily explain why the TD reduction was possible on the GaN/Si₃N₄ interface, providing additional GaN growth sites on the Si₃N₄ intermediate layer. We speculate that the 250°C higher growth temperature of the MOCVD enables the inter-diffusing behavior of the regrown GaN layer. Additionally, during the cooling process, thermal shrinkage critically damaged the crystallized Si₃N₄ layer, and thereby severe cracks were formed. Note that the CTE of the GaN, Si₃N₄, and quartz are 5.6, 3.3, and $0.3 \times 10^{-6} \text{ K}^{-1}$, respectively. In detail, during the MBE growth, the 1st GaN layer was epitaxially formed on the Si₃N₄ layer at a growth temperature of 800°C. At this time, most of the deformations were generated at the most outer 1st GaN layer, which resulted in the severe cracks of the 1st GaN layer. Next, during the MOCVD growth, the growth temperature was 250°C higher compared to the MBE growth temperature, and as a result, Ga inter-diffusion happened from the 1st GaN layer to the Si₃N₄ layer. Then, the crystallized Si₃N₄ layer suffered from strong tensile strain due to the large thermal mismatch with the quartz substrate during the cooling step. Considering the MOCVD cases, voids were found, which is possibly due to the faster growth of neighboring grains as well as cracks during cooling. It is observed that the planar 2nd GaN layer had vivid threading dislocations (TD) from the top of the 1st GaN to the 2nd GaN layer as well as bunches of defects; these are shown in Fig. 6(b). Meanwhile, the SAG- 2nd GaN layer showed rather reduced TDs, as seen in Fig. 6(c). Despite the reduction of TDs in the SAG- 2nd GaN layer, elongated lateral defects were formed on planes parallel to the substrates, as shown in one selected red-dashed rectangle in Fig. 6(c). In a vast number of cases, these are accepted as basal-plane stacking faults (BSF). Fig. 6(d)–6(f) display selected area diffraction (SAD) patterns of the 1st GaN layer, planar 2nd GaN layer, and SAG- 2nd GaN layer, respectively. Most of polycrystalline properties were proved by the ring-like patterns of the 1st GaN layer (Fig. 6(d)). Quasi-discrete spots on the ring-like pattern

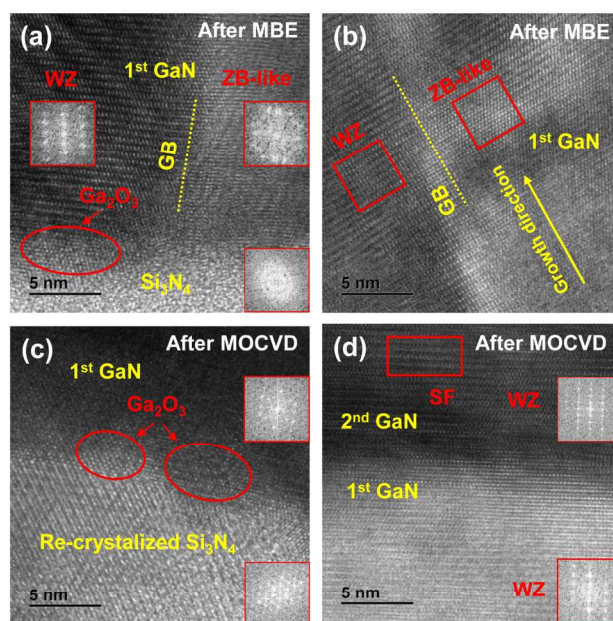


Fig. 7. High resolution TEM images and corresponding FFT patterns (insets) of (a) 1st GaN layer at near Si₃N₄ layer, (b) middle grain-to-grain, (c) 1st GaN layer at near re-crystallized Si₃N₄ layer, (d) interface between 1st GaN and planar 2nd GaN. Polycrystalline properties were observed at grain-to-grain interfaces for all samples. The clarity of the FFT pattern became vivid after conducting MOCVD growth, indicating improved crystallinity. Red-lined rectangles show defects in grains and red circles show Ga₂O₃ regions with mixed structure.

are caused by the twisted in-plane orientation of the neighboring grains. Fig. 6(e) shows the SAD pattern of the planar 2nd GaN layer in the middle of a grain. A single crystalline wurzite GaN was confirmed by the clear six-fold symmetry. This indicates that the enlarged GaN grown by MOCVD effectively increases the crystalline quality, but the single crystalline properties are only effective within a single micrometer-sized grain. The SAG- 2nd GaN layer also showed single crystallinity in the middle of a grain (Fig. 6(f)). Hence, we believe that much smaller scale local epitaxy such as nano-scale mask patterns might open more chances to improve a quality of crystal arrays.

To understand the growth evolution of the GaN on an amorphous layer, it is important to investigate the structural properties of the interfaces, e.g., grain-to-grain and layer-to-layer. First, Fig. 7(a) and 7(b) show high-resolution (HR) images of the 1st GaN layer at near Si₃N₄ layer and middle grain-to-grain after MBE growth. Here, we could observe the direct evidence Ga₂O₃ nanoclusters on Si₃N₄ layer, as discussed from EDX characterization in Fig. 3. The insets of Fig. 7(a) show fast Fourier transformation (FFT) on local regions, displaying dispersed FFT patterns from the crystalline disorder induced by defects and twisted orientation. For example, the Si₃N₄ underlying layer has a quite blurred FFT patterns, indicating amorphous properties without any re-crystallization during MBE growth. Meanwhile, different atomic arrangements on the left and right side of the grain boundary (GB) were

found as wurtzite (WZ) and partial zinc blende (ZB-like) structures. Much clear evidence of these mixed crystal features was observed around GB on the middle of 1st GaN in Fig. 7(b), where WZ and ZB-like atom stacking was seen in the red box. After MOCVD re-growth, on the other hand, Si₃N₄ region became re-crystallized, as shown in hexagonal arrangement of HR image as well as FFT patterns (bottom) in Fig. 7(c). It might be attributed to deep inter-diffusion, indicating that Ga atoms from the 1st GaN layer were diffused into the Si₃N₄ layer.²⁶ We still could find Ga₂O₃ regions with a mixed structure, as shown in the upper FFT patterns in Fig. 7(c). Fig. 7(d) shows the HR TEM images taken from the interface between 1st GaN and 2nd GaN. Although the spots of the planar 2nd GaN layer were clearer than those of the 1st GaN layer, a high density of stacking-fault-like defects were also identified by dispersed FFT pattern (inset of Fig. 7(d)).

IV. Optical properties and residual strain

To prove the spatial arrangement of crystallinity, cathodoluminescence (CL) was carried out. Fig. 8(a) shows a cross-sectional SEM image of the planar 2nd GaN layer. Its spatial CL images were also exhibited by panchromatic (Fig. 8(b)) and monochromatic views (Fig. 8(c)). No luminescence was observed at the 1st GaN layer due to low crystallinity caused by the high density of defects. In contrast, randomly local areas formed on the 2nd GaN layer showed near-band-edge emission. As proved from the TEM images in Fig. 6, GB and TD can play important roles as non-radiative recombination centers at the interfaces. The weak emission of the monochromatic CL image at 3.42 eV indicates that the planar 2nd GaN layer has poor crystal quality. Fig. 8(d) shows the spot-

mode CL spectra of each position from P1 to P4, as shown in Fig. 8(a). No distinguishing emission was measured around the 1st GaN layer (P1) and 2nd GaN layer (P2). In contrast, near-band-edge emission (3.44 eV) was observed in the middle of the microscale-size grain (P3 and P4). The dominance of the shorter emission energy at 3.37 eV and the emission broadening is possible due to the high density of BSF mixtures such as I₁-, I₂-, and E-BSF.²⁷ On the other hand, Fig. 8(e) shows a cross-sectional SEM image of the SAG- 2nd GaN layer. Its panchromatic (Fig. 8(f)) and monochromatic (Fig. 8(g)) CL images also appeared in the same manner as the planar 2nd GaN layer. Emissive regions were clearly expanded in comparison to the planar 2nd GaN layer. Spread growth from opened window to the both outsides was observed in the bending manner. This bending behavior clearly reduces TDs, as reported elsewhere, thereby enhancing band-edge emission distribution in Fig. 8(g).²⁸ Fig. 8(h) exhibits the spot-mode CL spectra of each position from S1 to S2, as shown in Fig. 8(e). No emissive regions (S1) existed at GB on the window opening. Above the masking area, band-edge emission at 3.43 eV was dominantly identified, which was slightly redshifted due to a weak tensile strain caused by SAG. It was also found that there is high density of BSF mixtures from the peak broadening at around 3.35 eV, where I₂ BSF is prominent. However, the intensity of the band-edge emission was higher than that of the BSF centers as well as the planar 2nd GaN layer, which indicates that SAG was a quite effective growth method for improving the crystal quality. Therefore, growth competition in nature between neighboring grains can be controlled even on the GaN on amorphous substrate.

XRD measurement could provide us further reliable

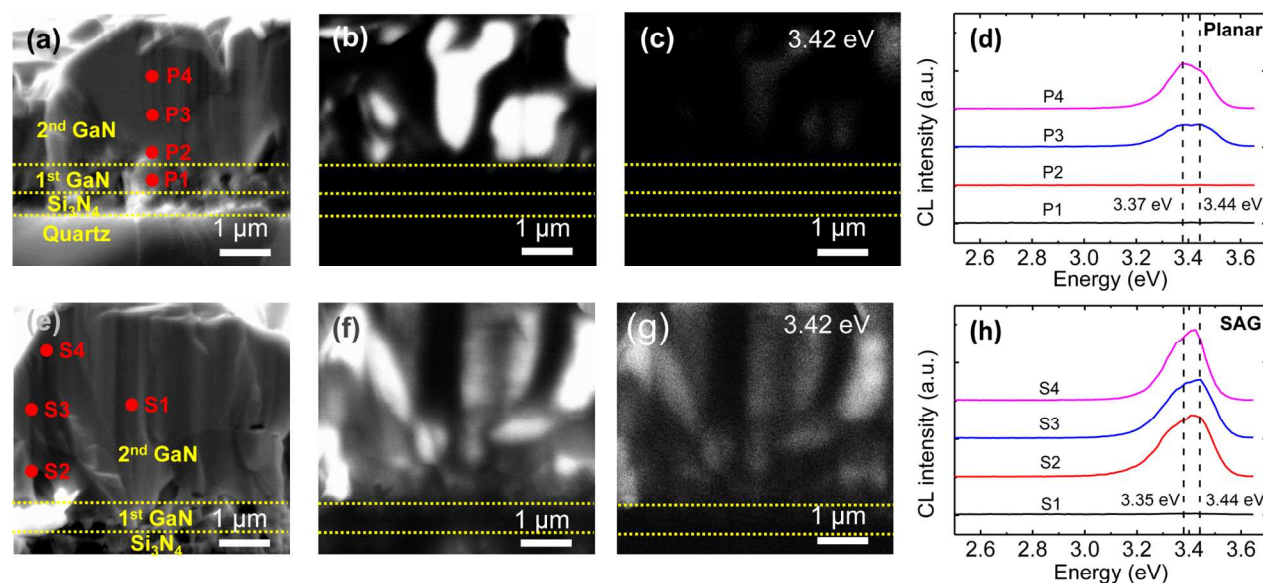


Fig. 8. (a) Cross-sectional SEM image of planar 2nd GaN. Its corresponding (b) panchromatic- and (c) monochromatic CL emission images. (d) Spot mode CL spectra measured on P1–P4 in Fig. 8(a). (e) Cross-sectional SEM image of selective 2nd GaN. Its corresponding (f) panchromatic- and (g) monochromatic CL emission images. (h) Spot mode CL spectra measured on S1–S4 in Fig. 8(e).

examination of crystalline properties. Fig. 9(a) shows 2θ -scans of grown samples, where dominant peaks were detected at 34.8° , corresponded to (0002) orientation. Two other satellite peaks placed at around 32° and 45° are representative of the 1st GaN layer, indicating (10 $\bar{1}$ 0) orientation and reflection (asterisk) from the aluminium sample holder. This indicates that the 1st GaN contains a few mixed-orientations, as discussed in Fig. 7. However, when we grew the 2nd GaN layer by MOCVD, the satellite peaks found in 2θ -scans had almost vanished, and instead, the signal intensity of the peak corresponding to (0004) was highly enhanced and the peak was observed as a family of the (0002) peak. In addition, the full width at half maximum (FWHM) of the regrown 2nd GaN layer became narrower than that of the 1st GaN layer. Hence, the combined epitaxy with the MOCVD and MBE certainly contributes to the crystal ordering, shown as the selection of the preferred orientation along the c -axis direction as well as improved crystal quality.

The effect of strain on epitaxial growth is also of importance

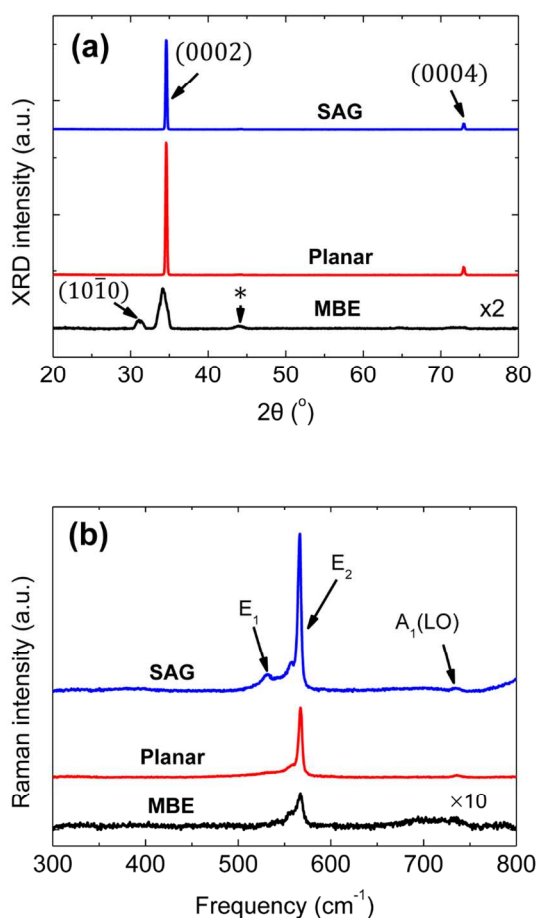


Fig. 9. (a) XRD 2θ -scans and (b) Raman spectra of grown layers. Slightly mixed orientation of the 1st GaN became (0002) orientation by growing with the MOCVD growth step. Strain was fully relaxed on the 1st GaN and planar GaN, while the SAG – 2nd GaN suffered from slight tensile strain.

since it could be related to wafer bowing, e.g., a large CTE mismatch results in severe cracks due to huge tensile strain, as can be seen in typical GaN/Si. Raman spectra can exhibit the remaining strain of the top layer for the 1st GaN and 2nd GaN layers, as shown in Fig. 9(b). Note that the E_2 mode is related to displacement in the c -plane, and the $A_1(\text{LO})$ mode comes from atomic relative motions along the c -axis direction.²⁹ The E_2 peak was observed at 567.2 cm^{-1} in both the 1st GaN and planar 2nd GaN layers. Since this indicates a nearly strain-free state ($567 \pm 0.1 \text{ cm}^{-1}$), residual stresses in the 1st GaN and planar 2nd GaN layer were negligible. For the SAG- 2nd GaN layer, the E_2 peak was located at 566.6 cm^{-1} , indicating the slight tensile strain of 0.161 GPa, using the relation $\sigma = \Delta\omega/4.3 \text{ cm}^{-1}$.³⁰ Hence, the lateral growth enhancement by SAG affected the degree of strain in the GaN layer, in a manner quite similar to other reports elsewhere.²⁸ The emergence of E_1 at 532 cm^{-1} is presumably attributed to the stripe morphology of the SAG- 2nd GaN layer since the E_1 mode of the Raman spectra can be over-susceptible from surface geometry.^{30,31} The $A_1(\text{LO})$ peaks also reflect strain status in a similar manner. The $A_1(\text{LO})$ peak of the planar 2nd GaN layer is located at 736 cm^{-1} without dispersion properties, and this is well matched with the strain-free GaN layer ($736.5 \pm 0.2 \text{ cm}^{-1}$), while the $A_1(\text{LO})$ peak of the selectively grown GaN layer is at (734.1 cm^{-1}), indicating slight tensile strain by the short Raman frequency shift.³⁰ However, broad dispersion is shown in the 1st GaN layer. It is speculated that peak broadening is attributed to unintentional inter-diffusion of Si atoms from Si_3N_4 to the 1st GaN layer at the interface. Due to the coupling of the LO phonon to the overdamped plasmon, the $A_1(\text{LO})$ peak was broadened and almost vanished with the increase in Si concentration of the 1st GaN by inter-diffusion.³²

V. Polarity study from chemical etching

Although both the planar and SAG- 2nd GaN exhibited c -plane dominant orientation from XRD measurement, it is required to be studied in more detail since the grown structures are composed of distorted microstructural grains. Hence, the grown samples were dipped into 3M KOH solution at 80°C . Fig. 10(a) and 10(b) display the surface morphology of 1st GaN after KOH etching. The procedure revealed that grain boundaries tend to be etched and hexagonal grains were almost remained. Note that N-polar GaN typically suffers from a strong chemical reaction compared to the Ga-polar GaN, and thereby is rapidly etched.³³ It indicates that individual grains usually have Ga polarity, whilst the grain boundaries have N exposed polarity. This is quite well matched with the TEM observation from the Fig. 7(a) and 7(b), where ZB-like structures were frequently found at the grain-to-grain interfaces. Furthermore, top surfaces of the each grain were partially etched, indicating that the middle of grain has slightly mixed polar properties despite Ga-polar dominance

Fig. 10(c) and 10(d) exhibit the surface morphology of the SAG- 2nd GaN after KOH etching. The morphology of grains was changed to pyramid-like shape including several needle-like structures corresponded to inversion domains (IDs) (Fig.

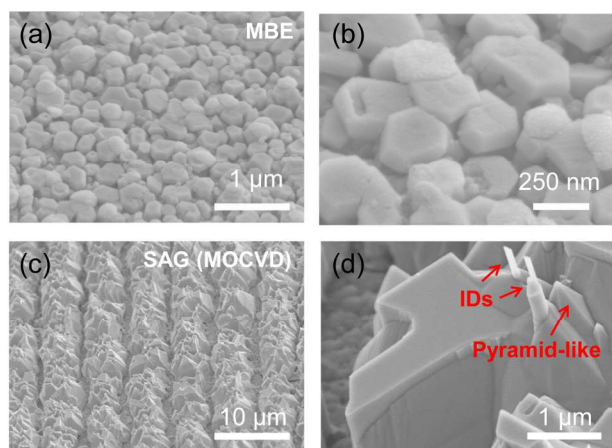


Fig. 10. SEM images of (a) 1st GaN grown by MBE, (b) its zoomed image, (c) SAG- 2nd GaN, and (d) its zoomed image after chemical etching in the KOH solution. 1st GaN hexagonal grains were almost remained, but grain boundaries tend to be etched. SAG- 2nd GaN shows well defined pyramid-like shape with columnar defects of IDs.

10(d)).³⁴ It was also revealed that N exposed regions were strongly etched. We have observed that the several microscale grains were stacked, where the grain interfaces might be easily mixed polarity as well as nonradiative components. Hence, these distorted grains might be easily etched during the KOH solution. Some needle-like IDs were also an evidence of local Ga polarity. Generally IDs come from the interface to layer surface with narrow and straight columnar structure. This

caused by growth rate difference between Ga- and N-polar GaN. Having a higher growth rate, Ga-polar GaN propagate to entire surface from interface and emerged at the centers of opposite N-polarity areas. After dipping KOH solution, it is expected that Ga-polarity IDs are etched much slower than surrounding areas of N-polarity. Finally, Ga-polarity IDs have straight and narrow columnar shape, whilst rest of the areas changed to pyramidal shape.^{34–36}

Note that conventional Ga-polar GaN layer is grown on Al covered surface of AlN buffer layer or sapphire (Al₂O₃) substrate. At the interface, higher bonding energy of Al-N (compared with Ga-N) determines Ga polarity of GaN by its bonding configuration. In this case, N polarity is kinetically unfavorable on the Al contained surface.^{14,37} On the other hand, N polarity can be induced without Al platform.³⁸ In our case, 1st GaN could be clustered on Ga₂O₃ depleted regions, i.e., around Ga₂O₃ nanoclusters on Si₃N₄, thereby inducing N polarity as shown as the results of KOH etching for 1st GaN. In addition, N-polar GaN could be further grown during the MOCVD growth since the adjacent grains do not have ordered height, thereby polarity inversion could be induced as a result of coalescence.³⁹ Therefore, we could conclude that the 2nd GaN has mixed polarity with Ga- and N-polar GaN, where the N polarity was usually enhanced around grain boundaries.

VI. Proposed growth model and further prospects

Based on the analysis of GaN on amorphous layer so far, here we propose growth model, as illustrated in Fig. 11. Although it

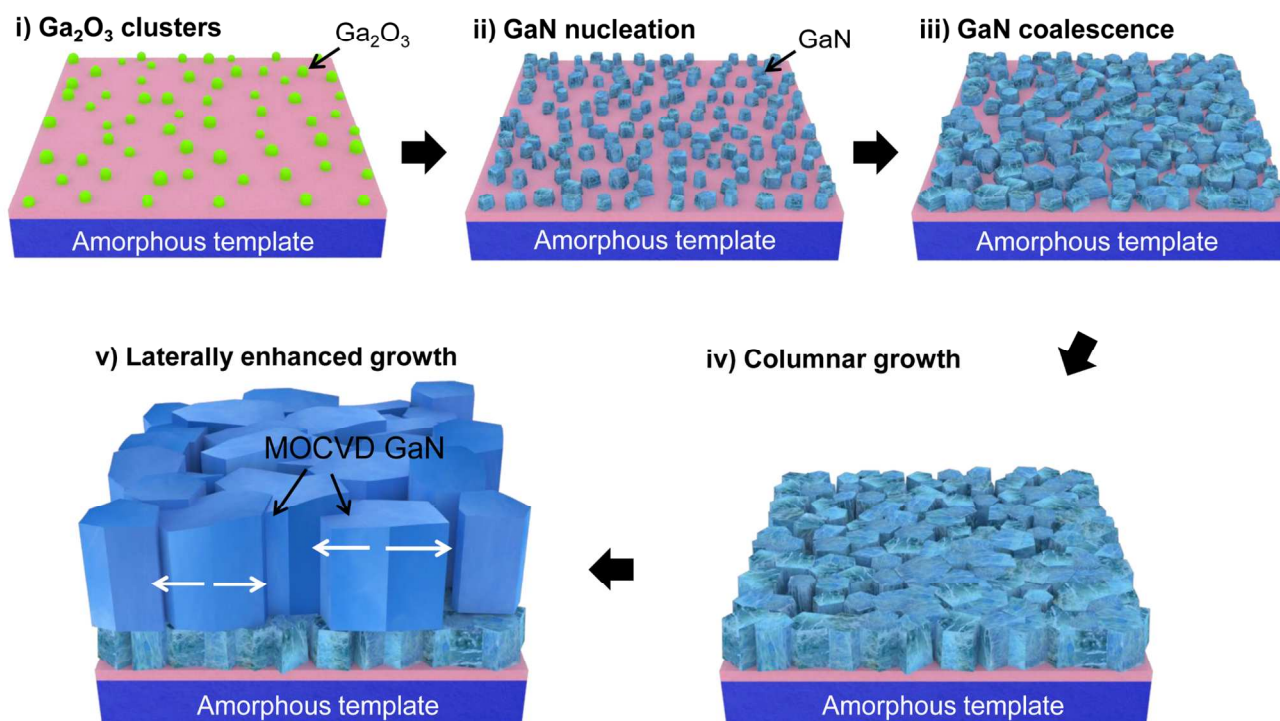


Fig. 11. Schematics of the growth model and procedures i) Ga₂O₃ clustering, ii) GaN nucleation, iii) local GaN coalescence, iv) columnar growth via MBE, and v) laterally enhanced growth via MOCVD.

has intentionally exaggerated for our purpose, we believe that it might be quite helpful to understand the results showed in this study as well as to improve the crystal quality. The procedures are simply described in Fig. 11 as follows; i) Ga₂O₃ clustering, ii) GaN nucleation, iii) local GaN coalescence, iv) columnar growth via MBE, and v) laterally enhanced growth via MOCVD. The origin of O source at the beginning of GaN growth is not clear at this time. We speculate that it might be attributed to native oxide on the Si₃N₄/quartz sample surface. Due to chemical reaction Si₃N₄ and quartz in HF solution, conventional cleaning process using HF solution should have been avoided in sample preparation step, thereby that native oxides might not be fully removed during thermal cleaning process in MBE chamber. Finally Ga₂O₃ nanoclusters are formed on the surface after Ga exposures. Then, Ga-polar GaN was formed usually on the Ga₂O₃, while N-polar GaN mainly is originated from the direct GaN clustering on the amorphous surface. The nitridation was performed at a rather longer time (1 hour), higher plasma power (350 W), and also higher substrate temperature (700°C) than the one for a typical nitridation process and epitaxy growth on sapphire or GaN template.¹⁰ As a result, it can provide strong N₂ reactivity, forming initial GaN clusters on the amorphous Si₃N₄ layer.²¹ These clusters on the amorphous interface became N-polar GaN seeds on non-Ga₂O₃ regions, i.e., around Ga₂O₃ nanoclusters. Then, local coalescence occurs among GaN nucleators since their distances are quite close by < 100 nm. Further nanocolumns were formed by MBE growth, where the grown structures were governed by VW growth mode, thereby columnar growth happened.^{40–42} Finally, one large grain was formed on these several nanocolumns and further lateral growth was enhanced by MOCVD. When edges of individual grain keep preferred orientation, enlarged planar grain was formed with six-fold hexagonal geometry. Whereas the edges do not have coherent angles, it results in distorted grains with grain boundaries where mixed crystal structures are frequently happened. In case of MOCVD growth, it reduces the mixed crystal structures such as wurtzite and zinc blende mixtures, but also has single crystalline features in the middle of microstructures.

As evident from these findings, we could suggest two approaches to improve crystal qualities of GaN on amorphous layer. One is to deposit (or insert) new preferred orientation layer before the growth to induce coherent grain edges. By considering material parameters such as in-plane lattice and thermal stabilities, Ti, Hf, and graphenes could be good candidates to be satisfied as reported elsewhere.^{19,43–45} These preferred orienting layers can not only induce single crystalline grain, but also be enabled to grow further enlarged 2D layer. The other approach is to grow nanowire structures by using smaller hole-shaped array such as nanoscale SAG. Recently, there have been several reports to improve crystal quality by the nanoscale epitaxy and for the realization of actual device.^{26,46} These nanoscale SAG can be quite of interests for the GaN on amorphous SAG since single crystalline microstructure could be demonstrated as evident in this study. Furthermore, this

array-type GaN nanowire can suffer from much less biaxial strain than that of 2D films since they are grown only on small localized regions.

Conclusion

A two-stage combined epitaxy was carried out with MBE and MOCVD to grow GaN on an amorphous layer. To obtain adoptable layer on any amorphous substrates, Si₃N₄ layer is deposited and quartz substrate is used as a thermally durable substances. The 1st GaN layer growth via MBE provided an epitaxial buffer layer composed of hundreds-of-nanometer scale grains with planar surface morphology. Despite the polycrystalline properties of the 1st GaN layer, it has a highly preferred orientation along *c*-plane on amorphous. The 2nd GaN layer growth via MOCVD improved the crystalline properties with a few micrometer scale grains. Mixed polarity of grown GaN was identified by XRD measurement as well as KOH chemical treatment. By changing growth tools, the growth mode was also changed from VW mode to SK mode, thereby increasing the growth rate and reducing the density of the grain boundary. This approach resulted in a strong and extended band-edge emission of the SAG- 2nd GaN layer within a micro-sized grain, indicating single crystalline quality, while high defect densities such as stacking faults and threading dislocations were found for the planar 2nd GaN layer. High resolution TEM study was also performed at grain-to-grain and layer-to-layer interfaces. These characterizations could give us a much deeper understanding regarding the availability of single crystalline GaN on novel amorphous substrates. Therefore, it could be a guide to grow much improved single crystals on other substances for the realization of optoelectronic GaN-based devices in the near future.

Acknowledgements

This research was supported by Basic Science Research Program through the National Research Foundation of Korea (NRF) funded by the Ministry of Education (NRF-2013R1A1A2A10006632) and the Core Technology Development Program for Next-generation Energy of Research Institute for Solar and Sustainable Energies (RISE), GIST.

Author Contribution

Jung-Wook Min^a and Si-Young Bae^b contributed equally to this work.

Notes and references

^a Department of Physics and Photon Science, Gwangju Institute of Science and Technology, Gwangju, 500-712, Republic of Korea

^b Department of Electrical Engineering and Computer Science, Nagoya University 466-8550, Japan

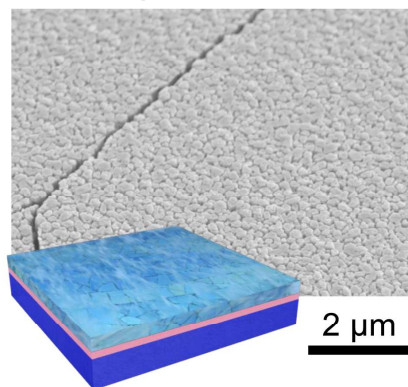
^c School of Material Science and Engineering, Gwangju Institute of Science and Technology, Gwangju 500-712, Republic of Korea

- ^d Advanced Photonics Research Institute, Gwangju Institute of Science and Technology, Gwangju, 500-712, Republic of Korea
- ^e School of Information and Communications, Gwangju Institute of Science and Technology, Gwangju 500-712, Republic of Korea
- 1 M. R. Krames, O. B. Shchekin, R. Mueller-Mach, G. O. Mueller, L. Zhou, G. Harbers and M. G. Craford, *J. Disp. Technol.*, 2007, **3**, 160–175.
 - 2 S. Pimpurkar, J. S. Speck, S. P. DenBaars and S. Nakamura, *Nat Photon*, 2009, **3**, 180–182.
 - 3 D. Zhu, D. J. Wallis and C. J. Humphreys, *Rep Prog Phys*, 2013, **76**, 106501.
 - 4 M. A. Green and M. J. Keevers, *Prog. Photovolt. Res. Appl.*, 1995, **3**, 189–192.
 - 5 S. Inoue, K. Okamoto, T. Nakano, J. Ohta and H. Fujioka, *Appl. Phys. Lett.*, 2007, **91**, -.
 - 6 K. Yamada, H. Asahi, H. Tampo, Y. Imanishi, K. Ohnishi and K. Asami, *Appl. Phys. Lett.*, 2001, **78**, 2849–2851.
 - 7 P. Hageman, J. Schermer and P. Larsen, *Thin Solid Films*, 2003, **443**, 9–13.
 - 8 M. Hiroki, H. Asahi, H. Tampo, K. Asami and S. Gonda, *J. Cryst. Growth*, 2000, **209**, 387–391.
 - 9 S.-E. Park, D.-J. Kim, S. Woo, S.-M. Lim and B. O. J. *Cryst. Growth*, 2002, **242**, 383–388.
 - 10 T. Araki, H. Kagatsume, T. Noguchi, T. Maruyama and Y. Nanishi, *Phys. Status Solidi C*, 2003, **0**, 200–204.
 - 11 S. Fan, S. Zhao, X. Liu and Z. Mi, *J. Vac. Sci. Technol. B*, 2014, **32**, -.
 - 12 W. C. Hughes, W. H. R. Jr, M. a. L. Johnson, S. Fujita, J. W. C. Jr, J. F. Schetzina, J. Ren and J. A. Edmond, *J. Vac. Sci. Technol. B*, 1995, **13**, 1571–1577.
 - 13 G. Nouet, P. Ruterana, H. Tampo and H. Asahi, *J. Phys. Condens. Matter*, 2002, **14**, 12697.
 - 14 K. Xu, N. Yano, A. Jia, A. Yoshikawa and K. Takahashi, *Phys. Status Solidi B*, 2001, **228**, 523–527.
 - 15 A. Konar, A. Verma, T. Fang, P. Zhao, R. Jana and D. Jena, *Semicond. Sci. Technol.*, 2012, **27**, 024018.
 - 16 M. H. Wong, Y. Pei, T. Palacios, L. Shen, A. Chakraborty, L. S. McCarthy, S. Keller, S. P. DenBaars, J. S. Speck and U. K. Mishra, *Appl. Phys. Lett.*, 2007, **91**, -.
 - 17 J.-Y. Chang and Y.-K. Kuo, *J. Appl. Phys.*, 2012, **112**, -.
 - 18 S. Keller, N. A. Fichtenbaum, M. Furukawa, J. S. Speck, S. P. DenBaars and U. K. Mishra, *Appl. Phys. Lett.*, 2007, **90**, -.
 - 19 J. H. Choi, A. Zoukarniev, S. I. Kim, C. W. Baik, M. H. Yang, S. S. Park, H. Suh, U. J. Kim, H. Bin Son, J. S. Lee, M. Kim, J. M. Kim and K. Kim, *Nat Photon*, 2011, **5**, 763–769.
 - 20 B. O. Jung, S.-Y. Bae, Y. Kato, M. Imura, D.-S. Lee, Y. Honda and H. Amano, *CrystEngComm*, 2014, **16**, 2273–2282.
 - 21 M. Zhong, F. Qin, Y. Liu, C. Wang, J. Bian, E. Wang, H. Wang and D. Zhang, *J. Alloys Compd.*, 2014, **583**, 39–42.
 - 22 B. Leung, J. Song, Y. Zhang and J. Han, *Adv. Mater.*, 2013, **25**, 1285–1289.
 - 23 A. B. Rahane, M. D. Deshpande and S. Chakraborty, *J. Phys. Chem. A*, 2012, **116**, 10559–10565.
 - 24 S. S. Kumar, E. J. Rubio, M. Noor-A-Alam, G. Martinez, S. Manandhar, V. Shutthanandan, S. Thevuthasan and C. V. Ramana, *J. Phys. Chem. C*, 2013, **117**, 4194–4200.
 - 25 M. Haerberlen, D. Zhu, C. McAleese, M. J. Kappers and C. J. Humphreys, *J. Phys. Conf. Ser.*, 2010, **209**, 012017.
 - 26 J. H. Choi, E. H. Cho, Y. S. Lee, M. Shim, H. Y. Ahn, C. Baik, E. H. Lee, K. Kim, T. Kim and S. Kim, *Adv. Opt. Mater.*, 2014, **2**, 302–302.
 - 27 J. Lähnemann, U. Jahn, O. Brandt, T. Flissikowski, P. Dogan and H. T. Grahn, *ArXiv14051261 Cond-Mat*, 2014.
 - 28 Y. Kato, S. Kitamura, K. Hiramatsu and N. Sawaki, *J. Cryst. Growth*, 1994, **144**, 133–140.
 - 29 M. S. Liu, L. A. Bursill, S. Praver, K. Nugent, Y. Tong and G. Zhang, *Appl. Phys. Lett.*, 1999, **74**, 3125–3127.
 - 30 C. Kisielowski, J. Krüger, S. Ruvimov, T. Suski, J. Ager III, E. Jones, Z. Liliental-Weber, M. Rubin, E. Weber and M. Bremser, *Phys. Rev. B*, 1996, **54**, 17745.
 - 31 S. Nagarajan, O. Svensk, M. Ali, G. Naresh-Kumar, C. Trager-Cowan, S. Suihkonen, M. Sopanen and H. Lipsanen, *Appl. Phys. Lett.*, 2013, **103**, -.
 - 32 T. Kozawa, T. Kachi, H. Kano, Y. Taga, M. Hashimoto, N. Koide and K. Manabe, *J. Appl. Phys.*, 1994, **75**, 1098–1101.
 - 33 D. Zhuang and J. H. Edgar, *Mater. Sci. Eng. R Rep.*, 2005, **48**, 1–46.
 - 34 J. Jasinski, Z. Liliental-Weber, Q. S. Paduano and D. W. Weyburne, *Appl. Phys. Lett.*, 2003, **83**, 2811–2813.
 - 35 V. Potin, P. Ruterana and G. Nouet, *Mater. Sci. Eng. B*, 1999, **59**, 173–176.
 - 36 L. T. Romano, J. E. Northrup and M. A. O'keefe, *Appl. Phys. Lett.*, 1996, **69**, 2394–2396.
 - 37 A. Yoshikawa and K. Xu, *Thin Solid Films*, 2002, **412**, 38–43.
 - 38 M. Stutzmann, O. Ambacher, M. Eickhoff, U. Karrer, A. Lima Pimenta, R. Neuberger, J. Schalwig, R. Dimitrov, P. J. Schuck and R. D. Grober, *Phys. Status Solidi B*, 2001, **228**, 505–512.
 - 39 J. Song, G. Yuan, K. Xiong, B. Leung and J. Han, *Cryst. Growth Des.*, 2014, **14**, 2510–2515.
 - 40 V. Consonni, M. Hanke, M. Knelangen, L. Geelhaar, A. Trampert and H. Riechert, *Phys. Rev. B*, 2011, **83**, 035310.
 - 41 T. Stoica, E. Sutter, R. J. Meijers, R. K. Debnath, R. Calarco, H. Lüth and D. Grützmacher, *Small*, 2008, **4**, 751–754.
 - 42 R. K. Debnath, R. Meijers, T. Richter, T. Stoica, R. Calarco and H. Lüth, *Appl. Phys. Lett.*, 2007, **90**, 123117.
 - 43 K. Okamoto, S. Inoue, T. Nakano, J. Ohta and H. Fujioka, *J. Cryst. Growth*, 2009, **311**, 1311–1315.
 - 44 T. Araki, S. Uchimura, J. Sakaguchi, Y. Nanishi, T. Fujishima, A. Hsu, K. K. Kim, T. Palacios, A. Pesquera, A. Centeno and others, *Appl. Phys. Express*, 2014, **7**, 071001.
 - 45 J. W. Shon, J. Ohta, K. Ueno, A. Kobayashi and H. Fujioka, *Sci. Rep.*, 2014, **4**.
 - 46 K. Kishino, K. Nagashima and K. Yamano, *Appl. Phys. Express*, 2013, **6**, 012101.

Table of contents

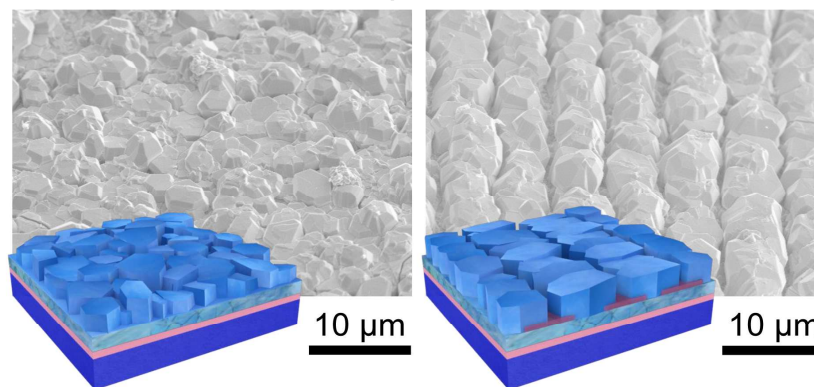
To achieve an epitaxial GaN layer on an amorphous substrate, we developed a method of two-stage combined epitaxial growth using molecular beam epitaxy (MBE) and metal-organic chemical vapor deposition (MOCVD). The first MBE growth step provided us effective nucleation with uniform morphology. Meanwhile, the second MOCVD growth enabled improved crystalline quality.

MBE grown 1st GaN



On amorphous SiN_x/quartz substrate

MOCVD regrown 2nd GaN



Planar growth was performed on bare 1st GaN template without mask formation (left) and SAG was performed on stripe patterned surface of 1st GaN (right)